Available online at www.sciencedirect.com

ScienceDirect

Ceramics International 40 (2014) 1829–1834

CERAMICS INTERNATIONAL

www.elsevier.com/locate/ceramint

Microstructure and mechanical properties of ZrO_2 ceramics toughened by 5–20 vol% Ta metallic particles fabricated by pressureless sintering

A. Smirnov*, J.F. Bartolomé

Instituto de Ciencia de Materiales de Madrid (ICMM), Consejo Superior de Investigaciones Científicas (CSIC), C/ Sor Juana Inés de la Cruz 3, 28049 Madrid, Spain

Received 19 April 2013; received in revised form 16 July 2013; accepted 17 July 2013
Available online 24 July 2013

Abstract

ZrO_2-based composites toughened by 5, 10, 15 and 20 vol% lamellar shape Ta metallic particles were made by pressureless sintering. The microstructure and mechanical properties of these novel ceramic–metal composites have been studied. With only 15 vol%, the toughness of ZrO_2–Ta composites was increased from 9.1 of monolithic zirconia to 14 MPa $m^{1/2}$ and the average bend strength was 700 MPa. Our results have demonstrated that zirconia transformation and ductile phase toughening concepts can get together to enhance the fracture toughness of zirconia-based materials with high strength.

Keywords: B. Composites; C. Mechanical properties; C. Toughness and toughening; Microstructure

1. Introduction

In the past few years, the use of ceramic materials has significantly increased in various applications due to the unique characteristics of these materials in comparison with metals and polymers. The advantageous properties of ceramic materials are hardness, rigidity, abrasive resistance and low density. Zirconia is an interesting ceramic material because it has good mechanical properties. This effect is based on the tetragonal to monoclinic phase transformation under an applied stress. This stress-induced martensitic transformation is associated with a volume increase of approximately 3–5%. A transformation zone is created as a crack propagates through the ceramic and a shielding stress is exerted on the crack. This reduces the local stress intensity level at the crack tip, and thus improves the fracture toughness of the material [1]. Nevertheless, the major limitation of zirconia based ceramics is their low crack resistance properties. Brittle ceramics can be toughened by introducing a ductile phase into them. The increase of the fracture toughness depends on the amount, size and shape of the metal phase and on the uniformity of their distribution [2–9]. Several studies on zirconia reinforced with metals such as nickel, stainless steel, molybdenum and niobium have been reported in the literature [10–17]. Moreover, metal particles in a ceramic matrix disperse the energy of propagating cracks due crack bridging mechanism and as a result increase the fracture toughness of the material. Other mechanisms which bring about the dispersion of fracture energy are (a) deflection of crack path by particles, (b) branching of cracks and (c) stress relaxation via crack nucleation or local plastic flow [18]. Consequently, these mechanisms can interact with each other and, under certain circumstances, the interaction is synergistic [19].

Tantalum was selected as the metal second phase because of its biocompatibility, corrosion resistance, and mechanical properties [20–23]. Metals usually exhibit higher coefficient of thermal expansion, thereby further complicating the problem of adherence to an oxide material. However, in this particulate system, the average coefficient of thermal expansion of Ta in the range 20–1000 °C is 6.5×10^{-6} °C^{-1}, is lower compared to a value of 12×10^{-6} °C^{-1} for 3Y-TZP. Thus, when this composite is

*Corresponding author. Tel.: +34 91 3348 990; fax: +34 91 372 0623.
E-mail address: tusluk@smail.ee (A. Smirnov).

0272-8842/$ - see front matter © 2013 Elsevier Ltd and Techna Group S.r.l. All rights reserved.
http://dx.doi.org/10.1016/j.ceramint.2013.07.084

cooled from the sintering temperature, the reinforcement contracts less than the matrix, which results into compressive stress in the metal particles.

In previous work, zirconia–Ta composite was fabricated by hot pressing [24]. Hot pressing sintering, spark plasma sintering or pulse electric current sintering are typical techniques employed to produce ceramic–metal composites. However, many of these techniques are not economically viable depending on the use of the final product. Thus, conventional sintering is still a more attractive sintering method to produce ceramic products, mainly due to its simplicity and cost compared to other methods.

The purpose of the present study was to obtain dense 3Y-TZP/Ta composites by conventional sintering (CS) and describe the influence of tantalum particles on the mechanical properties of zirconia–tantalum composites with different amounts of metal phase.

2. Experimental procedure

2.1. Starting materials

The following commercially available powders have been used as raw materials: (1) tetragonal zirconia polycrystals (3Y-TZP, 3 mol% Y_2O_3; TZ-3YE, Tosoh Corp.), with an average particle size of $d_{50}=0.26\pm0.05$ μm, a BET specific surface area of 16 ± 3 m^2/g. (2) Tantalum (Alfa Aesar, 99.97% purity) with an average particle size $d_{50}=44$ μm.

Tantalum powder was attrition-milled with zirconia balls in a teflon container for 4 h using isopropilic alcohol as liquid media. The ball-milled resulting powder consists of flake-like deformed Ta particles with a high aspect ratio and a mean particle size of 42 μm.

2.2. Powder processing

Zirconia/Ta suspensions of 80 wt% solid content were prepared using distilled water as liquid media and a 3 wt% addition of an alkali-free organic polyelectrolyte as surfactant [5]. Four powder mixtures compositions with the following ZrO_2 to Ta ratio (in vol%): $95ZrO_2$/5Ta, $90ZrO_2$/10Ta, $85ZrO_2$/15Ta and $80ZrO_2$/20Ta were prepared. The mixture was homogenized by milling with zirconia balls in polyethylene containers at 150 rpm during 24 h and then dried at 90 °C during 12 h. The resulting powders were ground in an agate mortar and subsequently passed through a 75 μm sieve. The mixed powders were cold isostatically pressed to cylindrical green samples (≈9 mm in diameter and 50 mm in length) at 200 MPa and sintered in argon atmosphere at 1500 °C for 2 h before being cooled down to room temperature. Heating and cooling rate 5 °C/min was used.

2.3. XRD characterization

The X-ray diffraction analyses (XRD) of these samples were carried out in a Bruker D8 diffractometer using CuKα ($\lambda=1.5405981$ Å) radiation working at 40 kV and 30 mA in a step-scanning mode from 27° to 33 ° with a step size of 0.01° and a scan speed of 0.06 deg/min. The monoclinic phase content of different surfaces was calculated using the Garvie and Nicholson method [25]

$$X_m=\frac{I_m(111)+I_m(\bar{1}11)}{I_m(111)+I_m(\bar{1}11)+I_t(111)}$$

where, I_t and I_m represent the integrated intensity (area under the peaks) of the tetragonal $(101)_t$ and monoclinic $(111)_m$ and $(-111)_m$ peaks. The monoclinic volume fraction was then obtained using equation proposed by Toraya et al. [26]

$$V_{mtot}=\frac{1.311X_m}{1+0.311X_m}$$

2.4. Microstructural and mechanical characterization

The microstructure of sintered specimens was studied on surfaces polished down to 1 μm and scanning electron microscopy (SEM, Phenom G2, Netherlands). The Vickers hardness, *Hv*, was measured using a Vickers diamond indenter (Leco 100-A, St. Joseph, MI) on polished surfaces, with applied load of 490 N with an indentation time of 10 s. The magnitude of the Vickers hardness was determined according to

$$Hv=1.854\,P/d^2,$$

where P is the applied load (in N) and d is the diagonal length (in mm). The corresponding indentations sizes were determined using the same scanning electron microscopy. The hardness results were averaged over 10 indentations per specimens.

2.4.1. Fracture toughness

Fracture toughness was measured using the single edge notched beam (SENB) on machined specimens in the form of bars with dimensions of $3.0\times4.0\times45$ mm^3. It should be noted that specimens from the same size were used for three point bending flexural test as well. The tests were performed at room temperature using a 5 kN universal testing machine SHIMADZU AutoGraph AG-X at a crosshead speed of 0.5 mm/min with span 40 mm. Notch was introduced by using diamond blade (saw) [24].

2.4.2. Three point bending flexural test

The tests were performed at room temperature using a universal testing machine (Shimadzu AutoGraph AG-X 5 kN, Japan) [27]. The specimens in the form of bars with dimensions of $3.0\times4.0\times45$ mm^3 were loaded to failure with a crosshead speed of 0.5 mm/min and a span of 40 mm. The strengths, σ_f, were calculated from the failure loads, F (N), and the specimen dimensions, using the equation

$$\sigma_f=\frac{3FL}{2bd^2}$$

where L is the length of the support span (mm), b is the width (mm) and d is the height (mm). The Young modulus was obtained from the slopes of load-deflection curves of three

point bending tests. A static extensometer was used to measure the deflection with an error in the measurement of 0.1%.

The density of sintered specimens was measured according to the Archimedes method.

3. Results and discussion

3.1. Microstructure

An electron micrograph of ZrO_2–Ta composite is shown in Fig. 1. In this micrograph the darker and bright phases are zirconia and tantalum grains, respectively. The interface between ZrO_2 and Ta was well bonded and no microcracks were observed. The tantalum particles are uniformly dispersed in the matrix.

The tantalum oxide (Ta_2O_5) is always present at the starting Ta powder surface as passivated oxide layer. The phase diagram for the zirconia-rich portions of the Ta_2O_5–ZrO_2 system [28] at temperatures in excess of 1400 °C indicates limited solubility of the pentavalent oxide in zirconia (~2 mol% $TaO_{2.5}$). However, co-doping with yttria has been observed to enhance their solubility in the tetragonal phase [29–31]. We assume that the entire passivated oxide layer is present in solid-solution (SS) after sintering and the fraction of Ta_2O_5 was lower than this limit of 2 mol% SS. No additional phases were detected.

The densities of the 3Y-TZP/Ta composites obtained by pressureless sintering are presented in Table 2. The density tests confirmed the possibility of obtaining high density (> 90% th.) 3Y-TZP/Ta composites.

3.2. Mechanical properties

Evaluation of Vickers hardness (H_V), toughness (K_{IC}), elastic modulus (E) and flexural strength (σ_f), together with densities measured are given in Table 1.

The hardness is rising with increasing ceramic phase content, from 5.4 for the 3Y-TZP/15Ta composition, to 7.9 for the 3Y-TZP/5Ta composition. A maximum strength of ~697 MPa was obtained for the 3Y-TZP/15Ta composite. The higher porosity of composition with 20% vol. Ta explains its poor mechanical performance. The presence of porosity generally has a negative influence on mechanical properties, since pores can cause stress concentration, resulting in low strength.

By analyzing the mechanical behavior of the composites (strength versus amount of metallic phase) it can be concluded that strength increases until an optimum point of embedded metal particles (3Y-TZP/15Ta) and from this point values decrease significantly.

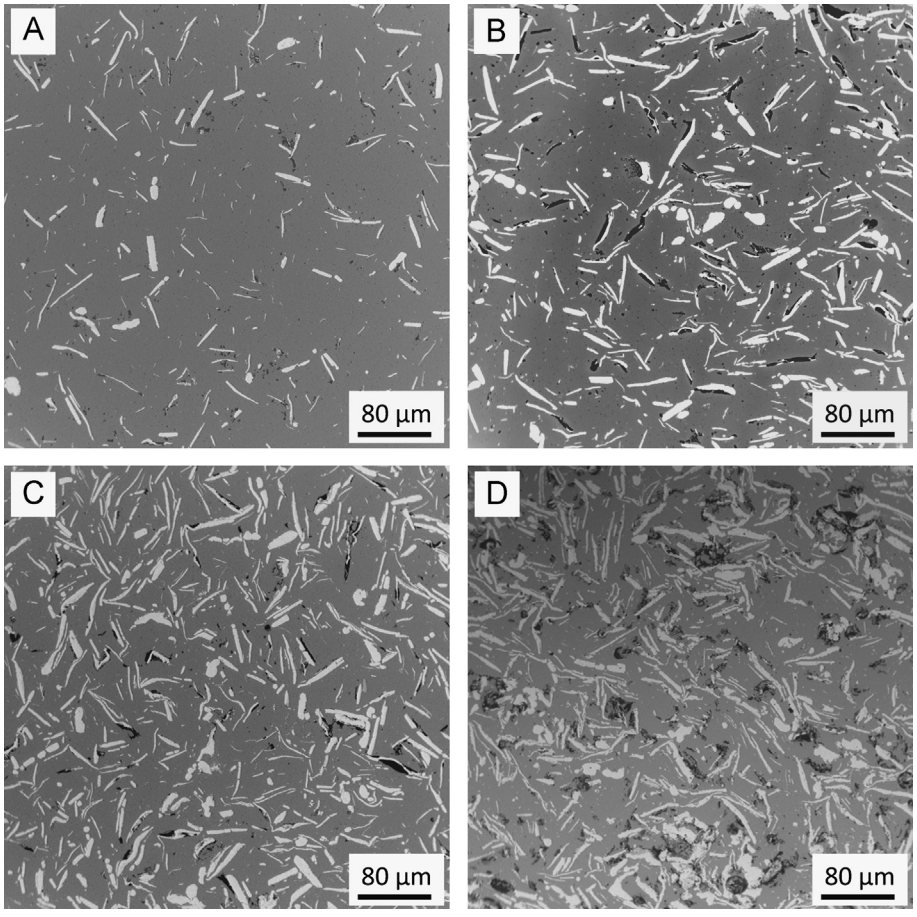

Fig. 1. SEM micrograph of microstructure in zirconia – (A) 5 vol%, (B) 10 vol% (C) 15 vol% and (D) 20 vol% Ta composite. Gray phase is zirconia; light is Ta and black is porosity.

Table 1
Mechanical properties and densities corresponding to the materials studied.

	3Y-TZP/5 Ta	3Y-TZP/10 Ta	3Y-TZP/15 Ta	3Y-TZP/20 Ta	3Y-TZP
Elastic modulus (GPa)	198 ± 5	191 ± 7	182 ± 8	136 ± 4	190 ± 8
Flexural strength (MPa)	438 ± 14	531 ± 17	697 ± 21	406 ± 12	787 ± 10
Vickers hardness (GPa)	7.9 ± 0.24	5.7 ± 0.31	5.4 ± 0.35	4 ± 0.36	4.8 ± 0.11
Toughness (MPa $m^{1/2}$)	12.1 ± 0.33	12.8 ± 0.42	14 ± 0.47	8.9 ± 0.44	9.1 ± 0.12
Density	96% th.	95% th.	95% th.	90% th.	98% th.

Table 2
The monoclinic volume fraction (V_{mtot}) for 3Y-TZP and 3Y-TZP/Ta composites.

	5 vol% Ta		10 vol% Ta		15 vol% Ta		20 vol% Ta		3Y-TZP	
	Polished surface	Fractured surface	Polished surface	Fractured surface	Polished surface	Fractured surface	Polished surface	Fractured surface	Polished surface	Fractured surface
V_{mtot}	3.7	17.2	3.9	19.1	4.2	28.5	3.8	15.2	1.1	10.2

The average fracture toughness of ceramic–metal composites was about 12–14 MPa $m^{1/2}$ (except the composition with 20 vol% Ta), which was higher than the result for the monolithic zirconia (about 9.1 MPa $m^{1/2}$). The increase in toughness may be due to the ductile metallic phase, which can absorb the energy of crack propagation during fracture, and could enhance crack deflection and bridging as well as stress relaxation near the crack tip. In addition, the increase in toughness occurred because of the presence of solid solution of Ta_2O_5 enhances the transformability of zirconia. Table 2 shows the monoclinic volume fraction for polished and fractured surfaces of monolithic zirconia and zirconia–metal composites. The obtained results showed that in the monolithic 3Y-TZP about 10 vol% of the tetragonal zirconia transformed to monoclinic symmetry during the failure. In the meantime, the analysis of XRD data proved that the fraction of zirconia transformation considerably increases for zirconia–metal composites. The enhanced transformability is related to the alloying effect on the tetragonality (c/a – cell parameters ratio) of stabilized tetragonal ZrO_2, so the addition of this oxide increases the tetragonal distortion of the cubic lattice. When a trivalent oxide, like Y_2O_3, is added to ZrO_2 as stabilizer, certain amount of lattice defects i.e. oxygen vacancies, are produced in the ZrO_2 lattice. The effect of doping with pentavalent oxides such as Ta_2O_5 (cationic radii in the +5 oxidation state ~0.68 Å) indicates that ions reside as substitutional defects in the zirconium lattice (ionic radius of the Zr^{4+} ion is 0.79 Å), annihilating the oxygen vacancies generated by yttria doping. Since oxygen vacancies are effective in stabilizing the tetragonal structures, the destabilizating effect of Ta doping can be attributed to the decreased concentration of oxygen vacancies. However it is important to underline that the composition with 20 vol% Ta demonstrates the lowest value of monoclinic volume fraction due to high porosity. The transformation toughening mechanism was expected to be considerably more effective in material with negligible porosity due to the magnitude of the *t–m* transformation.

Fractographic studies of the materials showed evidence of bridging and plastically deformed tantalum lamellar particles and matrix-reinforcement interfacial decohesion [Fig. 2]. Elongated thin Ta grains may act as bridges and deform plastically during the period of bending. On the other hand, the thick grains may act as elastic bridge and fail during the period of bending. Cleavage fracture indicates that the metal particles ultimately failed without much plasticity. Then the elastic and plastic deformation of the bridging particles before fracture contributes to a substantial toughening. Once the crack has reached the particle–matrix interface, the difference in the crack-tip opening displacement between the ductile particle and the brittle matrix will cause the crack to be locally blunted and its segments forced to circumvent the particle, thus bridging the crack along its length. On applying an external load to the sample, these ligaments impose closure traction on the crack surfaces against the opening of the crack. Thus, the bridging of intact ligaments reduces the stress at the crack tip through elastic loading and plastic deformation. So, the dominant toughening mechanism operating in the present ZrO_2–Ta composite is crack bridging, except the composition with 20 vol% Ta. In this particular case the dominant failure mechanism is metal particle pull-out. No evidence of plastic deformation was observed. Residual porosity remains at the ceramic–metal interface (Fig. 2D). Ceramic matrix composites reinforced with platelet or flake like particles, frequently show a considerable degree of porosity in the interface between the matrix and reinforcement phase. The sintering behavior of flake-reinforced composites may be compared to that observed in bimodal distribution of spherical particles [32]. Fine particles show rapid densification because of their high curvature, while the large particles (platelets or flakes) exhibit a lower driving force for sintering. Consequently, pore

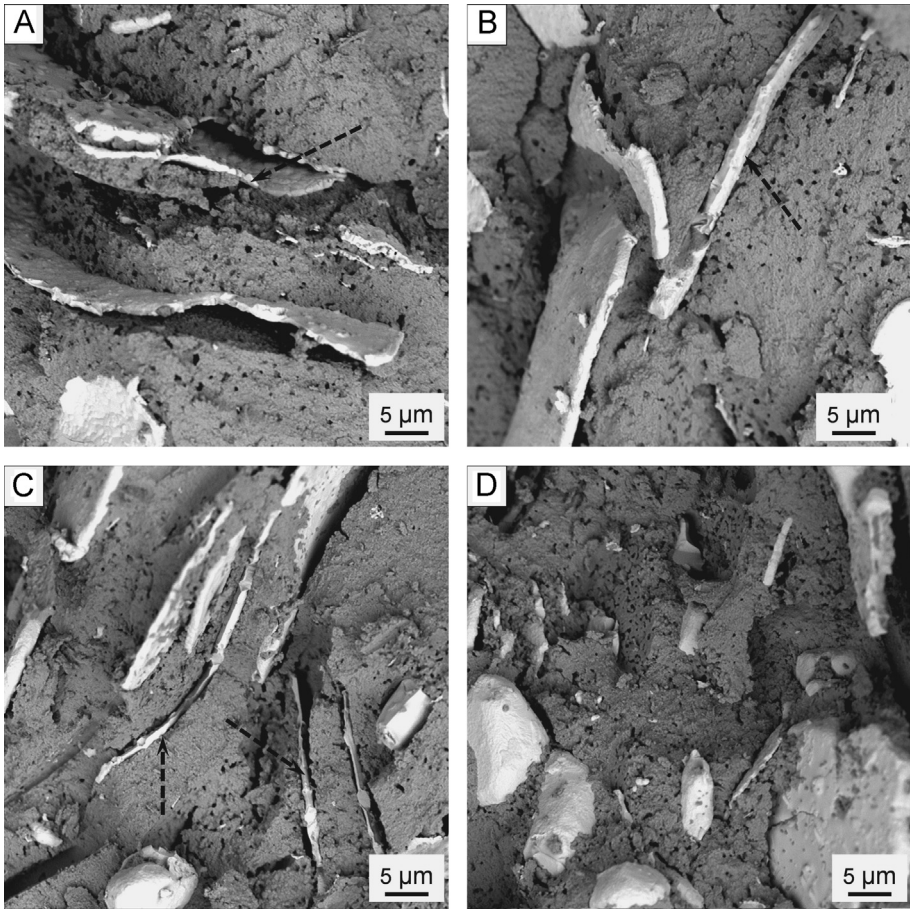

Fig. 2. SEM micrographs of the fracture surface of zirconia – Ta (A – 5 vol%, B – 10 vol%, C – 15 vol% and D – 20 vol%) composite. Dashed black arrows show the plastic deformation of tantalum particles.

channels between flake and dense fine-grained regions appear, and then the relative density of the compacts decreases when flakes amount are increased. This interface porosity enhances the formation of a weak boundary structure increasing the total probability of intergranular fracture. The metal particles begin to debond behind the crack tip and continue to debond as the crack extends (Fig. 2D). This debonding occurred by continuous decohesion with interaction with interface porosity.

The current results demonstrate that transformation and ductile phase toughening mechanisms can be successfully utilized together to enhance the fracture toughness of ceramic–metal composites fabricated by pressureless sintering. In this regard, the amount of second phase, due to the presence of intergranular porosity, can impart a low resistance to crack propagation and therefore, lower effectiveness of each toughening mechanism.

4. Conclusions

Homogeneous zirconia–metal composites (with 5, 10, 15 and 20 vol% Ta) were fabricated following a wet-processing route and pressureless sintering. All composites exhibited microstructures with uniformly distributed metallic particles into zirconia matrix. It was found that the addition of only 5, 10 and 15 vol% of Ta particles to the 3Y-TZP matrix, produces reinforcement effect which appears as increase of fracture toughness, 12.1 MPa $m^{1/2}$, 12.8 MPa $m^{1/2}$ and 14 MPa $m^{1/2}$, respectively. This increase in toughness was explained by crack bridging of the elastic–plastic deformations of ductile metal particles associated with the transformation toughening mechanism in zirconia matrix. The lower value in strength and fracture toughness of ZrO_2–20 vol% Ta composite is related to ceramic–metal interface porosity.

Acknowledgments

This work was supported by the Spanish Ministry of Science and Innovation (MICINN) under the Projects MAT2009-14542-C02-01 and MAT2012-38645. A. Smirnov has been supported by JAE-Pre Programme 2010.

References

[1] R. Stevens, Introduction to Zirconia and Zirconia Ceramics, Magnesium Electron Publication 56, 1986.
[2] V.D. Krstic, P.S. Nicholson, R.G Hoagland, Journal of the American Ceramic Society 64 (1981) 499.
[3] T. Rodriguez-Suarez, J.F. Bartolomé, J.S. Moya, Mechanical and tribological properties of ceramic/metal composites: a review of phenomena spanning from the nanometer to the micrometer length scale, Journal of the European Ceramic Society 32 (2012) 3887–3898.

[4] J.S. Moya, M. Díaz, C.F. Gutiérrez-González, L.A. Diaz, R. Torrecillas, J.F. Bartolomé, Mullite-refractory metal (Mo, Nb) composites, Journal of the European Ceramic Society 28 (2) (2008) 479–491.
[5] M. Diaz, J.F. Bartolomé, J. Requena, J.S. Moya, Wet processing of mullite/molybdenum composites, Journal of the European Ceramic Society 20 (20) (2000) 1907–1914.
[6] J.F. Bartolomé, C.F. Gutiérrez-González, R. Torrecillas, Mechanical properties of alumina–zirconia–Nb micro-nano-hybrid composites, Composites Science and Technology 68 (6) (2008) 1392–1398.
[7] T. Rodriguez-Suarez, S. Lopez-Esteban, J.F. Bartolomé, J.S. Moya, Mechanical properties of alumina-rich magnesium aluminate spinel/tungsten composites, Journal of the European Ceramic Society 27 (11) (2007) 3339–3344.
[8] K. Kameo, K. Friedrich, J.F. Bartolomé, M. Díaz, S. López-Esteban, J.S. Moya, Sliding wear of ceramics and cermets against steel, Journal of the European Ceramic Society 23 (15) (2003) 2867–2877.
[9] C.F. Gutiérrez-González, J.F. Bartolomé, Damage tolerance and R-curve behavior of Al_2O_3–ZrO_2–Nb multiphase composites with synergistic toughening mechanism, Journal of Materials Research 23 (02) (2008) 570–578.
[10] C. Pecharromán, J.I. Beltrán, F. Esteban-Betegón, S. López-Esteban, J.F. Bartolomé, M.C. Muñoz, J.S. Moya, Zirconia/nickel interfaces in micro- and nanocomposites, Materials Research and Advanced Techniques 96 (5) (2005) 507–514.
[11] J.S. Moya, S. López-Esteban, C. Pecharromán, J.F. Bartolomé, R. Torrecillas, Mechanically stable monoclinic zirconia–nickel composite, Journal of the American Ceramic Society 85 (8) (2002) 2119–2121.
[12] Y.G. Jung, S. Choi, C. Oh, U. Paik, Residual stress and thermal properties of zirconia/metal (nickel and stainless steel 304) functionally graded materials fabricated by hot pressing, Journal of Materials Science 32 (1997) 384–3850.
[13] C.F. Gutiérrez-González, A. Smirnov, J.F. Bartolomé, Aging effect on the tribological behavior of a novel 3Y-TZP/Nb biocomposite against ultra high molecular weight polyethylene (UHMWPE), Journal of the American Ceramic Society 95 (3) (2012) 851–854.
[14] Y. Yamada, A. Kawasaki, M. Taya, R. Watanabe, Effect of debonding at the phase interface on Young's modulus in sintered PSZ/stainless steel composites, Journal of the Japan Institute of Metals 58 (1994) 162–168.
[15] M. Nawa, K. Yamazaki, T. Sekino, K. Niihara, Microstructure and mechanical properties of 3Y-TZP/Mo nanocomposites—processing a novel interpenetrated intragranular microstructure, Journal of Materials Science 31 (1996) 2849–2858.
[16] S. López-Esteban, J.F. Bartolomé, C. Pecharromán, J.S. Moya, Zirconia/stainless-steel continuous functionally graded material, Journal of the European Ceramic Society 22 (16) (2002) 2799–2804.
[17] S. López-Esteban, J.F. Bartolomé, J.S. Moya, T. Tanimoto, Mechanical performance of 3Y-TZP/Ni composites: tensile, bending, and uniaxial fatigue tests, Journal of Materials Research 17 (7) (2002) 1592–1600.
[18] J.B Wachtman, Mechanical properties of ceramics, Wiley, New York, 1996.
[19] J.F. Bartolomé, C.F. Gutiérrez-González, C. Pecharromán, J.S. Moya, Synergistic toughening mechanism in 3Y-TZP/Nb composites, Acta Materialia 55 (17) (2007) 5924–5933.
[20] K.J. Welldon, G.J. Atkins, D.W. Howie, D.M. Findlay, Primary human osteoblasts grow into porous tantalum and maintain an osteoblastic phenotype, Journal of Biomedical Materials Research A 84 (3) (2008) 691–701.
[21] R. Godley, D. Starosvetsky, I. Gotman, Bonelike apatite formation on niobium metal treated in aqueous NaOH, Journal of Materials Science 15 (10) (2004) 1073–1077.
[22] H. Matsuno, A. Yokoyama, F. Watari, M. Uo, T. Kawasaki, Biocompatibility and osteogenesis of refractory metal implants, titanium, hafnium, niobium, tantalum and rhenium, Biomaterials 22 (11) (2001) 1253–1262.
[23] ASM Handbook, 10th ed., Materials Park, OH ASM International, 2000.
[24] A. Smirnov, J.F. Bartolomé, Mechanical properties and fatigue life of ZrO_2–Ta composites prepared by hot pressing, Journal of the European Ceramic Society 32 (2012) 3899–3904.
[25] R.C. Garvie, P.S. Nicholson, Phase analysis in zirconia systems, Journal of the American Ceramic Society 55 (6) (1972) 303–305.
[26] H. Toraya, M. Yoshimura, S. Somiya, Calibration curve for quantitative analysis of the monoclinic tetragonal ZrO_2 system by X-ray diffraction, Journal of the American Ceramic Society 67 (6) (1984) 119–121.
[27] ASTM C1161-02c(2008)e1, Standard Test Method for Flexural Strength of Advanced Ceramics at Ambient Temperature.
[28] PH100, ACerS-NIST Phase Equilibria Diagrams CD-ROM Database Version 3.1, 2005.
[29] Ta_2O_5–Y_2O_3–ZrO_2 system: experimental study and preliminary thermodynamic description, Journal of the European Ceramic Society, 31, 2011, pp. 249–257.
[30] D-J. Kim, Effect of Ta_2O_5, Nb_2O_5, and HfO_2 alloying on the transformability of Y_2O_3-stabilized tetragonal ZrO_2, Journal of the American Ceramic Society 73 (1) (1990) 115–120.
[31] D.-J. Kim, T.-Y. Tien, Phase stability and physical properties of cubic and tetragonal ZrO_2 in the system ZrO_2–Y_2O_3–Ta_2O_5, Journal of the American Ceramic Society 74 (12) (1991).
[32] J.P. Smith, G.L. Messing, Sintering of bimodally distributed alumina powders, Journal of the American Ceramic Society 67 (1984) 238–242.